Fe-Cr-Nb-B magnetic nanoparticles prepared by arc discharge for hyperthermia

I. MURGULESCU*, G. ABABEI, G. STOIAN, C. DANCEANU, N. LUPU, H. CHIRIAC
National Institute of Research and Development of Technical Physics, Iasi, Romania

$Fe_{67,7}Cr_{12}Nb_{0.3}B_{20}$ magnetic nanoparticles (MNPs) were studied for their applications in cancer treatment using hyperthermia. The aim of this paper is to determine if the arc discharge method can be used as an alternatively method to the long-time milling method of the amorphous ribbon for MNPs preparation for hyperthermia application. A correlation between working parameters and the magnetic properties of the arc discharge MNPs was establish. MNPs with dimensions between 5÷30 nm has been prepared. A similar thermo-magnetic behaviour of arc discharge MNPs versus milling particles was observed.

(Received March 5, 2019; accepted December 10, 2019)

Keywords: Arc discharge, Magnetic naonoparticles(MNPs), Hyperthermia

1. Introduction

Treatment of cancerous disease is one of the major development directions of modern medicine. Besides classical methods, based on chemotherapy and radiotherapy, different heating-based approaches are considered valuable. The cancer cells are considered to be more heat-vulnerable than the normal ones. A local temperature of 41÷47 °C initiate a cellular degradation mechanism in the tumours. However, after this value the healthy cells will be damaged. A heating process that does not elevate the temperature of the biological tissue above 45÷47°C can be carried out through magnetic hyperthermia [1]. These processes are conditioned by obtaining the amorphous structure in the FeCrNbB magnetic nanoparticles (MNPs) and the order of 20÷25nm size [2].

The specific magnetic behaviour of $Fe_{79.7-x}Cr_xNb_{0.3}B_{20}$ (x= 11÷13, at. %) glassy melt-spun ribbons with low Curie temperature, ranging from 290 to 330 K, depending on the Cr content, was investigated in previous works in experimental procedure [1-3] and theoretical approach [4-6], while the medical and biocompatibility implications have been studied and previously reported [7,8].

Conventionally, these MNPs are obtained by milling from amorphous ribbons to the desired particles size [1-3]. MNPs were obtained from various wet and dry milling method [7-8] or by chemical synthesis [9] but in crystalline state. The disadvantages of the conventional MNPs preparation method are related to the high milling time of 40÷200 hours and the possible presence of the surfactant (oleic acid or n-heptane) used for grinding to preserve glassy phase of the final product.

The aim of this article is to investigate the possibility of obtaining MNPs by other methods to eliminate the disadvantages of the classical method. The proposed method is the DC arc discharge. For this method, we want to establish correlations between the working parameters and the prepared MNPs properties.

From the category of alloys $Fe_{79.7-x}Cr_xNb_{0.3}B_{20}$ (x=11÷13, at. %) [1-3] we have chosen the middle of the interval (x=12 at. %) $Fe_{67,7}Cr_{12}Nb_{0.3}B_{20}$ to investigate the preparation possibilities.

2. Experiment

Arc discharge method allows the preparation of amorphous or crystalline particles with dimensions from few to hundreds of nanometres, depending on the depression of the inert gas and the parameters of the arc discharge.

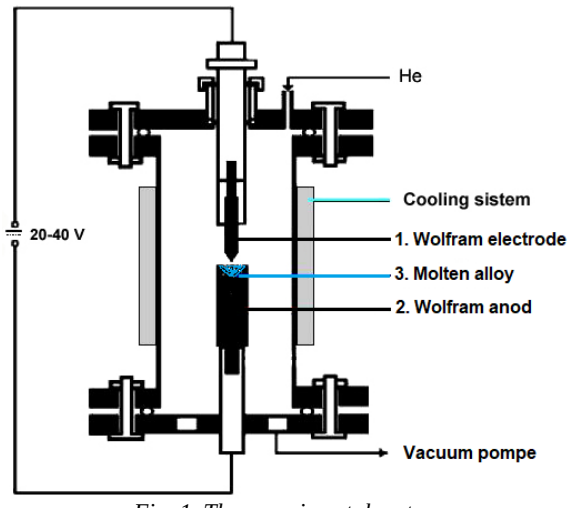

Fig. 1. The experimental system

The arc discharge methods is well known and used in different formulas and geometry [10-13] for producing spherical particles, filaments, nanotubes or fullerenes, and

in the last years used for biomedical applications [12-14]. Our experimental system is described in Fig. 1.

The electric arc was ignited between a wolfram electrode (1) and a water-cooled wolfram crucible (2) by high frequency initiator in a free inert gas (He). The bulk alloy (3) was heated and melted by the high temperature of the plasma; metal atoms were detached from the metal surface and evaporated into free atom state. Above the evaporation source there was a region filled with supersaturated metal vapours, where the metal atoms diffused around and collided each other to decrease the nuclei forming energy, as indicated in Fig. 2.

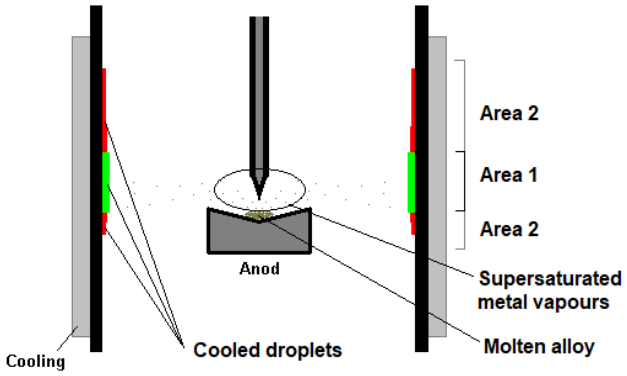

Fig. 2. Selective collection

When the metal vapour was supersaturated, a new phase was nucleated. The droplets were rapidly cooled and combined to form primary particles by an aggregation growth mechanism. The free inert gas convection developing between the hot evaporation source and the cooled collection cylinder has transported the particles out of this nucleation and growth region to the inner walls of the cylinder. The nanoparticles could be obtained after a period of passivation and stabilization (10 hours) in working gas and argon atmosphere.

$Fe_{67.7}Cr_{12}Nb_{0.3}B_{20}$ nanoparticles have been prepared by DC arc discharge method. The parameters used for the preparation of the $Fe_{67,7}Cr_{12}Nb_{0.3}B_{20}$ (at. %) powders are: temperature enclosure of 0 ºC to -17 ºC, working gas pressure of -0.85 to -0.5 bar He below the atmospheric pressure value, discharge current of 40 to 100 A, time discharge of 3 minutes to 15 minutes and the powders being collected from different areas of the enclosure. In the process of preparation, in the reaction chamber a vacuum of $2*10^{-4}$ mbar was realized and afterwards was backfilled with He atmosphere (purity 99.999%) at -0.4 ÷ -0.85 bar with respect to the atmospheric pressure.

The structural investigation of the arc discharge powder samples was carried out using the Bruker AXS D8 ADVANCE diffractometer, in the Bragg-Brentano configuration, geometry θ-θ, using the characteristic radiation Kα of copper (λ = 0.15418 nm), at a voltage of 40 kV and intensity of 40 mA, angular range 2θ = 30° ÷ 70°, speed 2 sec/step, scanning step: 0.02°. The quantitative and qualitative analysis of the phases present in the arc discharge MNPs was performed by interpreting the diffraction curves using the DIFFRACplus Eva program. Calculation of the crystallites/nanocrystallites size was achieved using Scherrer's relationship.

The magnetic behavior of the MNPs was studied using a Lakeshore vibrating sample magnetometer (VSM) in a maximum applied field of 4 T. The shapes, morphology and the dimensions of the nanoparticles were investigated by transmission electron microscopy (TEM) using Cs-corrected Libra operated at 200 kV and scanning electron microscopy (SEM) using a Neon40ESB microscope with energy dispersive X-ray (EDX) detector with energy resolution of 133eV.

3. Results and discussions

3.1. The effect of working parameters

To investigate the possibility of obtaining MNPs for applications in hyperthermia we studied the influence of each of the working parameters on their magnetic properties.

Selective collection. The major differences between our experimental system and the others [11, 13, 14] consist in powders collection zone. We found major qualitative differences in the magnetic properties of the particles deposited in different areas of the enclosure. In correlation with the flight time and the specific conditions of the arc discharge we find important differences between two deposition areas identified as follows: the area "1" at the same level of the electric arc that produces the evaporation and the area "2" above and below this zone (Fig. 2).

Particles with a short flying time will always be deposited in the "1" area according to the highest thermal gradient, but those with a long flying time can be deposited all over the place, both in zone "2" and in "1". These "1" and "2" areas cannot be completely separated and a slight diffusion of them will always be present.

Selective collection only in area "1" reduces the mass of prepared powders but increases its quality. Even small amounts of powder with the characteristics of area "2" may affect the characteristics of the collected material. This involves a certain scattering of experimental data. To investigate the thermomagnetic behaviour, we used a Vibrating Sample Magnetometer (VSM). Figure 3 shows the general magnetic behaviour of the collected powders: amorphous with nanocrystalline parts (green curve) from the area "1" and crystalline type from the area "2" (red curve). Next, we will expose this behaviour in correlation with the working parameters.

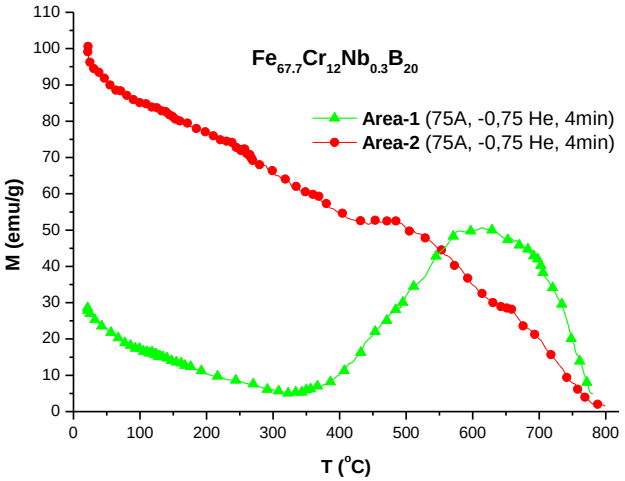

Fig. 3. Thermomagnetic curve obtained in the same arc discharge experiment for different collection areas

The experimental results presented in Fig. 4 show the reproducibility level of the magnetic properties despite the two areas' diffusion.

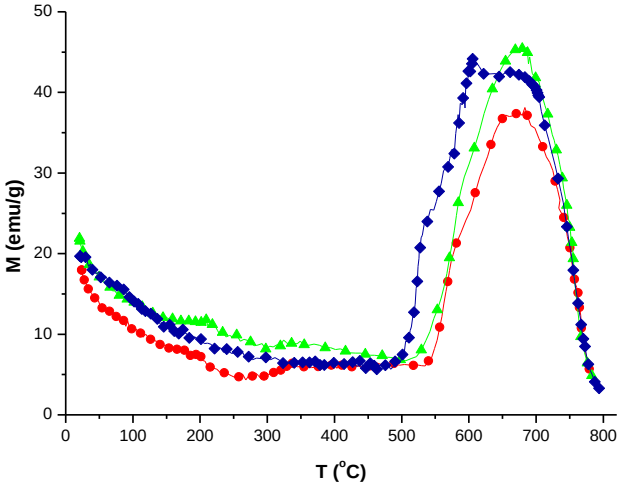

Fig. 4. Reproducibility of thermo-magnetically curve for different arc discharges MNPs having the same working parameters (70A, -0.7 bar He, 5 minutes)

Working pressure. The ideal thermomagnetic curve of an amorphous magnetic material shows a decrease of the magnetization to zero (obtained at Curie temperature), a bearing and an increase of the magnetization when the initialization temperature of the crystallization is reached, followed by a return to zero at the loss of magnetic properties.

In Fig. 5, the green curve is closest to the behaviour of the amorphous state. However, a very small fraction of crystalline material is present. The red and blue curves obtained for higher values of the working gas pressure show a percentage increase of the crystalline component.

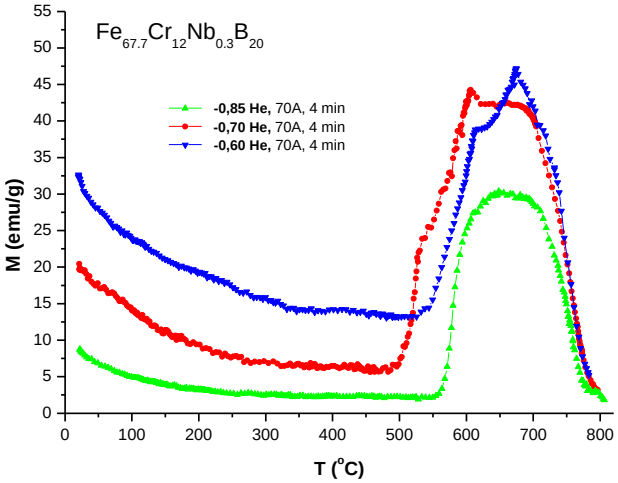

Fig. 5. Variation of the thermo-magnetic curves for different values of the working gas pressure

This behaviour is like that previously reported results [2] for different wet and dry grinding times. Regarding to the thermomagnetic curves, the particles obtained by the arc discharge are better than the particles obtained by dry milling, but inferior to those obtained by wet milling in oleic acid and reported in ref. [2].

The DC **discharge current** greatly defines the temperature of the electric arc. A correlation between the different discharge currents and the thermomagnetic curve was investigated (Fig. 6).

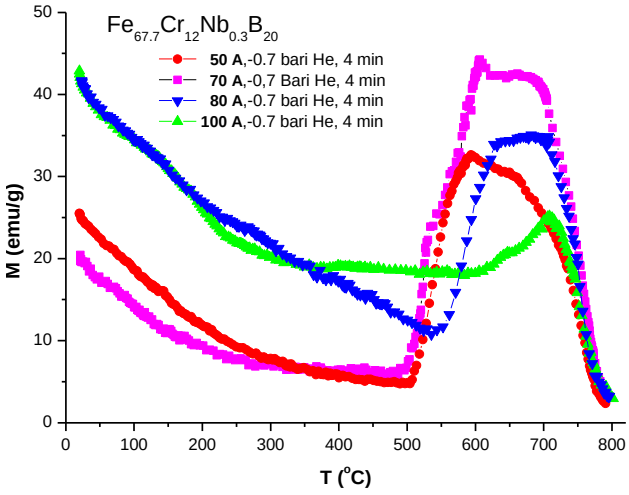

Fig. 6. Variation of the thermo-magnetic properties on the VSM curves for different values of the discharge current

The thermo-magnetic curves for values of the discharge current below to 70A are indicating a similar behaviour for predominant amorphous MNPs.

Above 70A discharge current, a crystalline behaviour of the thermo-magnetic curves is reached.

Deposition time. The increase in the amount of collected powder by increasing the deposition time was investigated (Fig. 7).

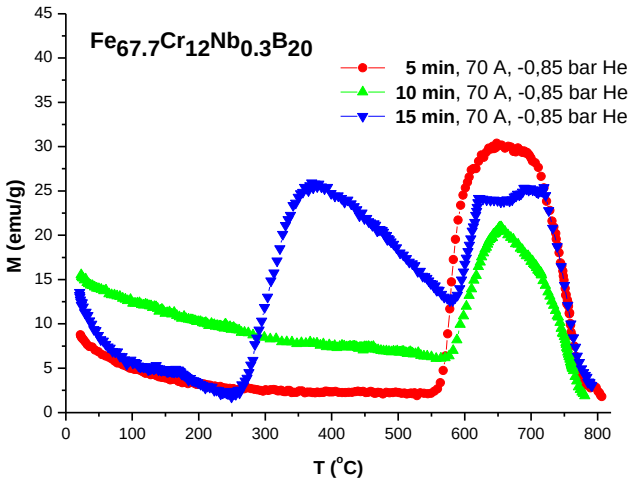

Fig. 7. The thermo-magnetic curves for different deposition times

For the same discharge parameters (70 A, -0.85 bar He), the increase in the deposition time of 5/10/15 minutes leads to a proportional increase in the amount of collected powder 4.2 / 8.1 / 12.7 mg from the area "1", but affecting the quality. In Fig. 7, the red curve (5 min deposition time) shows the appearance of a predominantly amorphous phase characteristic. The green curve (10 min deposition time) shows an increase of the crystalline fraction and the blue curve (15 min deposition time) shows even the appearance of a new phase with a new initialization temperature of the crystallization.

We consider that with the increase in the thickness of the deposited layer both the cooling rate of the particles at the moment of touching the wall and the thermal gradient decreases (the deposited powder representing a thermal insulating layer of the cooled enclosure), so the last deposited particles has a longer flight time than at the beginning of the arc discharge ignition. Changes on the thermo-magnetic curve may be due by altering the amorphous or nanocrystalline character of the powders. For this reason, we considered that for a good accuracy it is necessary to not exceed 5 minutes for a single discharge.

The deposited powder mass increase with the increasing of pressure, current and deposition time, but is limited at each of these parameters to preserve the glassy phase. Thus, with these limitations, we find that for a single arc discharge we can get only 8 mg of powder, in the used experimental geometry.

3.2. MNPs characterisation

The characterisation of MNPs was made using calorimetrical measurements, compositional (EDX), structural (X-ray) and size (SEM/TEM) investigations.

Calorimetric measurements. In order to use these powders in the treatment of cancerous tumours, it is necessary to obtain MNPs with the optimum heating temperature of 41÷47˚C. Their heating capacity was tested in the same system as other MNPs previously reported [7]. Thus, we used an experimental stand made from a 6-loop coil having a 46 mm internal diameter, fed by a RF generator 180-185 KHz, producing a magnetic field of 215 mT. Inside this coil is the powder sample dispersed in two millilitres of distillate water at a concentration of 10 mg/ml. This sample is thermally insulated from the environment and its temperature is measured with an optical thermometer with a precision of 1°C and the transmission of the signal was made by optical fibre.

For the $Fe_{67,7}Cr_{12}Nb_{0,3}B_{20}$ alloy, the measured heating temperature (temperature of self-controlled magnetic hyperthermia) varied for different working parameters in the 30÷42˚C range. For this reason we also investigated other compositions such as $Fe_{68.7}Cr_{11}Nb_{0.3}B_{20}$, $Fe_{69.7}Cr_{10}Nb_{0.3}B_{20}$, $Fe_{72.2}Cr_{7.5}Nb_{0.3}B_{20}$, $Fe_{74.7}Cr_5Nb_{0.3}B_{20}$. We obtained the best results, in terms of calorimetric measurements, for the $Fe_{71.2}Cr_{7.5}Nb_{0.3}B_{20}$ alloy for which we obtained values in the range of 40÷50˚C.

Table 1. The maximum RF heating temperatures obtained by calorimetric measurements

Alloy (at %)	T max [˚C]
Fe **Cr12** $Nb_{0.3}B_{20}$	30÷42
Fe **Cr11** $Nb_{0.3}B_{20}$	32÷39
Fe **Cr10** $Nb_{0.3}B_{20}$	33÷43
Fe **Cr7.5** $Nb_{0.3}B_{20}$	40÷50
Fe **Cr5** $Nb_{0.3}B_{20}$	47÷52

These values differ from Curie temperature measurements for massive alloys or powders obtained by milling of the amorphous ribbon, which may lead to the idea that powders obtained by DC arc discharge might not have exactly the same composition with the base alloy.

Composite uniformity was investigated by EDX. We investigated the values for the ratio of iron to chromium, knowing that the Curie temperature is reduced with the increase in chromium content. In the case of powders obtained by grinding the amorphous ribbon, the composite uniformity is within the limit of the measurement error of the method. The spread of measured data increases and the ratio of Fe and Cr changes in the case of MNPs obtained by arc discharge method. This means that in order to obtain nanoparticles with $Fe_{67,7}$ Cr_{12} $Nb_{0,3}B_{20}$ concentration we should use an initial alloy with $Fe_{72,2}$ $Cr_{7,5}$ $Nb_{0,3}B_{20}$ concentration.

A total of ten measurements were made for each investigated composition. MNPs with different compositions were obtained under the same working conditions (70A, -0.7 bar He, 5 min). The signal capture surface has an area of 1000 μm^2 (50 µm x 20 µm) and Magnification x 2K.

Table 2. EDX uniformity of the MNPs

Alloy (at %)	Minim Cr/Fe at %	Maxim Cr/Fe at %	**Cr/Fe** at % average
(MNPs by milling)			
$Fe_{67.7}Cr_{12}Nb_{0.3}B_{20}$	1/5.61	1/5.65	**1/ 5.65**
(MNPs by arc discharge)			
$Fe_{67.7}Cr_{12}Nb_{0.3}B_{20}$	1/3.06	1/3.38	1/ 3.22
$Fe_{72.2}Cr_{7,5}Nb_{0.3}B_{20}$	1/4.10	1/4.44	1/ 4.21
$Fe_{74.7}Cr_{5}Nb_{0.3}B_{20}$	1/8.03	1/8.82	1/ 8.38

These results are in good correlation with the calorimetric measurements mentioned above and are like other reported results for arc discharge synthesis of multicomponent nanoparticles [15], in which authors have reported deviations from the alloy composition of even particles sizes of 100 nm.

The structural characterization was performed by X-rays and the results shown in Figs. 8 and 9 are indicating that the structure of the samples is composed by a mixture of amorphous and nanocrystalline phases.

Although the techniques of interpretation of the X-ray spectra have undergone continuous improvements [16, 17], the simultaneous presence of the amorphous and nanocrystalline structures brings an additional difficulty in the correct evaluation of the different components.

The evaluation of the size crystallites was performed using the program Diffrac.Suite Eva, with Integral Breadt in the Scherrer relation, after Fourier Smooth.

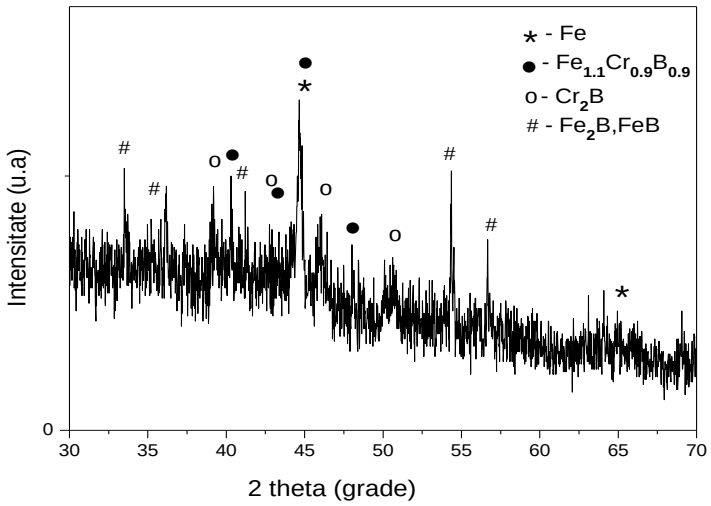

Fig. 8. Diffraction curve for the 50A discharge current [$Fe_{67,7}Cr_{12}Nb_{0.3}B_{20}$ alloy, 50A, -0.7 bar He, 5 min]

MNPs for the 50A discharge current [$Fe_{67,7}Cr_{12}Nb_{0.3}B_{20}$ alloy, 50A, -0.7 bar He, 5 min] present αFe-grain about 25-27 nm while all the other phases (Fe_2B, FeB, Cr_2B, $Fe_{1,1}Cr_{0,9}B_{0,9}$ phases) present grains with dimensions below 11 nm (Fig. 8).

For the 70A discharge current [$Fe_{67,7}Cr_{12}Nb_{0.3}B_{20}$ alloy, 70A, -0.7 bar He, 5 min] αFe-grain dimension is about 25-27 nm and 18-23 nm for the other phases (Fig. 9).

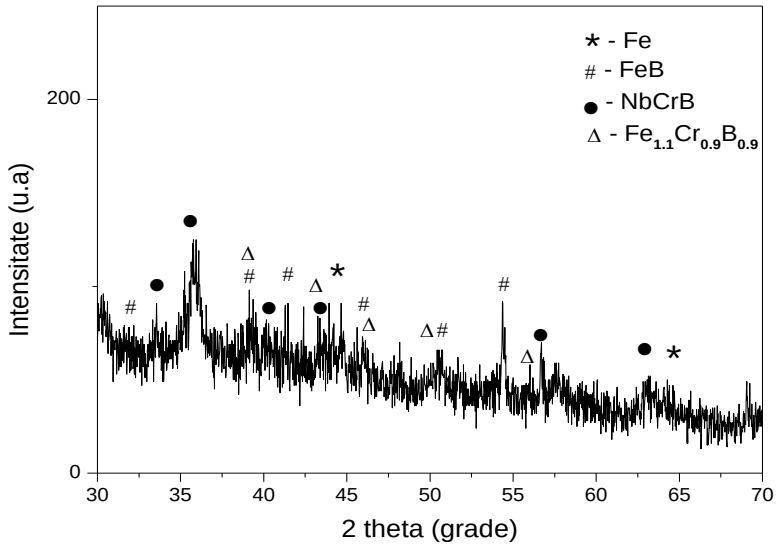

Fig. 9. Diffraction curve for 70A discharge current [$Fe_{67,7}Cr_{12}Nb_{0.3}B_{20}$ alloy, 70A, -0.7 bar He, 5 min]

In correlation with thermo-magnetic curves for different values of the discharge current we should limit the discharge current to 70A to keep the glassy phase of MNPs.

SEM (Scanning Electron Microscopy) image of MNPs is indicated in Fig. 10. The particles are small spheres (14.5nm diameter) self-arranged as filaments deposited on the cooled wall of the enclosure.

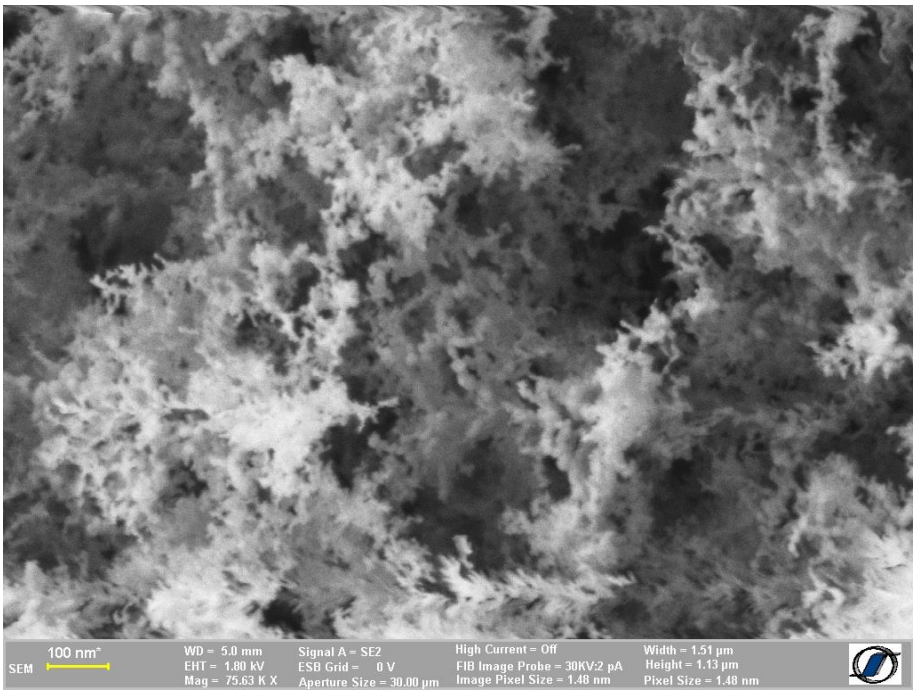

Fig. 10. Typical SEM (Scanning Electron Microscopy) image for MNP. Exemplification for $Fe_{67,7}Cr_{12}Nb_{0.3}B_{20}$ powders for arc discharge parameters [90A, -0,7 bar He, 4 min]

TEM (Transmission Electron Microscopy) investigation of particle sizes obtained at [80A, -0.7 bar He, 5 min] show in Fig. 11 an average value of 14.5 nm and a minimum of 8 nm for $Fe_{67.7}Cr_{12}Nb_{0.3}B_{20}$ MNPs.

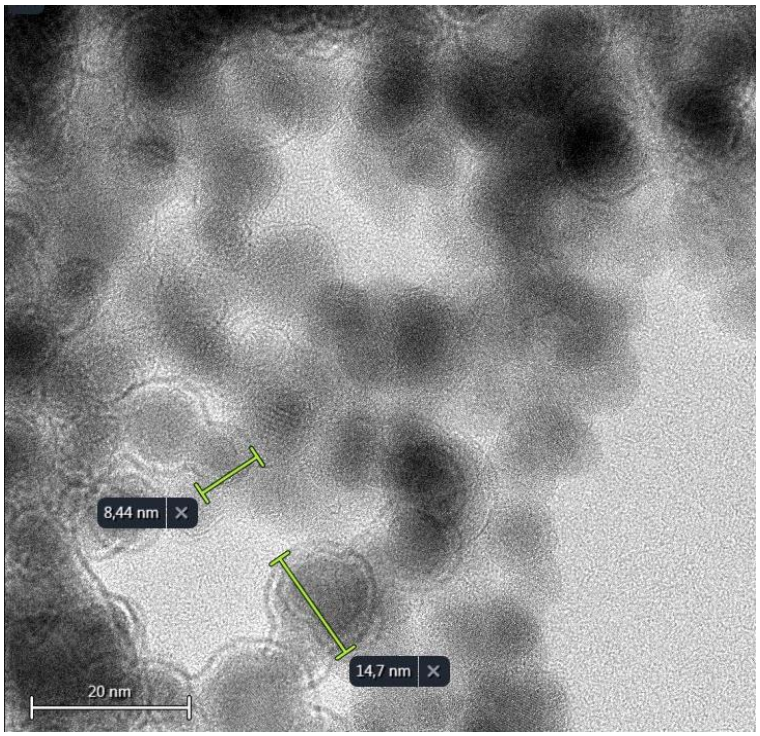

Fig. 11. Typical TEM image of MNPs. Exemplification for [$Fe_{67,7}Cr_{12}Nb_{0,3}B_{20}$ alloy, 80A, -0.7 bar He, 5min]

4. Conclusions

MNPs with dimensions of 5÷30 nm was prepared by the DC arc discharge method, highlighted by SEM, TEM and X-ray.

A correlation between working parameters and the magnetic properties of the arc discharge MNPs was establish.

In order to obtain nanoparticles with $Fe_{67,7}Cr_{12}Nb_{0,3}B_{20}$ concentration we should use an initial alloy into an arc discharge system with $Fe_{72,2}Cr_{7,5}Nb_{0,3}B_{20}$ at. % concentration. As a disadvantage of the method, at the nanometric level were observed fluctuations of the concentration of 10%.

A similar thermo-magnetic behaviour of arc discharge MNPs versus milling particles was observed. The MNPs prepared by the arc discharge have better magnetically and structural properties than the particles obtained by dry milling, but inferior to those obtained by wet milling in oleic acid [2], for the hyperthermia application.

Due to the fluctuations of the MNPs composition prepared by the arc discharge, the maximum heating temperature indicated by calorimetric measurement is not constant but varies within a temperature range.

References

[1] H. Chiriac, T. Petreus, E. Carasevici, L. Labusca, D. D. Herea, C. Danceanu, N. Lupu, Journal of Applied Physics **115**, 17B520 (2014).
[2] H. Chiriac, N. Lupu, M. Lostun, G. Ababei, M. Grigoraş, C. Dănceanu, Journal of Applied Physics **115**, 17B520 (2014).
[3] Ihab M. Obaidat, Bashar Issa, Yousef Haik, Nanomaterials **5**(1), 63 (2015).
[4] K. D. Bakoglidis, K. Simeonidis, D. Sakellari, G. Stefanou, M. Angelakeris, IEEE Transactions on Magnetics **48**(4), 1320 (2012).
[5] C. Gómez-Poloa), S. Larumbe, J. I. Pérez-Landazábal, J. M. Pastor, Journal of Applied Physics **111**, 07A314 (2012).
[6] I. Astefanoaei, H. Chiriac, A. Stancu, Journal of Applied Physics **121**, 104701 (2017).
[7] D. D. Herea, C. Danceanu, E. Radu, L. Labusca, N. Lupu, H. Chiriac, International Journal of Nanomedicine **13**, 5743 (2018).
[8] H. Chiriac, E. Radu, M. Țibu, G. Stoian, G. Ababei, L. Lăbușca, D. D. Herea, N. Lupu, Scientific Reports **8**, 11538 (2018)
[9] Lezhong Li, Xiaoxi Zhong, Rui Wang, Xiaoqiang Tu, Lei He, Optoelectron. Adv. Mat. **12**(3-4), 240 (2018).
[10] A. Szabó, C. Perri, A. Csató, G. Giordano, D. Vuono, J. B. Nagy, Materials **3**, 3092 (2010).
[11] J.-G. Lee, P. Li, C.-J. Choi, X.-L. Dong, Thin Solid Films **519**, 81 (2010).
[12] A. A. Ashkaran, Current Applied Phisycs **10**, 1442 (2010).
[13] B. Yanık, H. Agustos, Y. Ipek, A. Koyun, D. Uzunsoy, Arab J. Sci. Eng. **38**, 3587 (2013).
[14] S. Chaitoglou, M. R. Sanaee, N. Aguiló-Aguayo, E. Bertran, Journal of Nanomaterials **2014**, 178524 (2014).
[15] A. Mao, H. Xiang, X. Ran, Y. Li, X. Jin, H. Yu, X. Gu, Journal of Alloys and Compounds (2018), doi: https://doi.org/10.1016/j.jallcom.2018.10.170.
[16] E. Hermann, O. G. Duliu, M. Iovea, J. Optoelectron. Adv. M. **20**(7-8), 410 (2018).
[17] A. Chelmus, R. Radvan, L. Ghervase, Optoelectron. Adv. Mat. **12**(5-6), p. 314 (2018).

*Corresponding author: imurgulescu@phys-iasi.ro